DOI: 10.1002/chem.200700820

Evidence for Significant Through-Space and Through-Bond Electronic Coupling in the 1,4-Diphenylcyclohexane-1,4-diyl Radical Cation Gained by Absorption Spectroscopy and DFT Calculations

Hiroshi Ikeda,*[a] Yosuke Hoshi,[b] Hayato Namai,[b] Futoshi Tanaka,[b] Joshua L. Goodman,[c] and Kazuhiko Mizuno[a]

Abstract: Photoinduced single-electron-transfer promoted oxidation of 2,5-diphenyl-1,5-hexadiene by using *N*-methylquinolinium tetrafluoroborate/biphenyl co-sensitization takes place with the formation of an intense electronic absorption band at 476 nm, which is attributed to the 1,4-diphenylcyclohexane-1,4-diyl radical cation. The absorption maximum (λ_{ob}) of this transient occurs at a longer wavelength than is expected for either the cumyl radical or the cumyl cation components. Substitution at the *para* positions of the phenyl groups in this radical cation by CH_3O, CH_3, F, Cl, and Br leads to an increasingly larger redshift of λ_{ob}. A comparison of the ρ value, which was obtained from a Hammett plot of the electronic transition energies of the radical cations versus σ^+, with that for the cumyl cation shows that the substituent effects on the transition energies for the 1,4-diarylcyclohexane-1,4-diyl radical cations are approximately one half of the substituent effects on the transition energies of the cumyl cation. The observed substituent-induced redshifts of λ_{ob} and the reduced sensitivity of λ_{ob} to substituent changes are in accordance with the proposal that significant through-space and -bond electronic interactions exist between the cumyl radical and the cumyl cation moieties of the 1,4-diphenylcyclohexane-1,4-diyl radical cation. This proposal gains strong support from the results of density functional theory (DFT) calculations. Moreover, the results of time-dependent DFT calculations indicate that the absorption band at 476 nm for the 1,4-diphenylcyclohexane-1,4-diyl radical cation corresponds to a SOMO-3→SOMO transition.

Keywords: absorption · density functional calculations · electron transfer · orbital interactions · radical ions

Introduction

Observation of short-lived transients by absorption spectroscopy is a powerful methodology to elucidate the mechanisms of photoinduced electron-transfer (PET) reactions.[1] Usually the assignment of structures to the transients is accomplished by comparing the observed absorption spectra with those of intermediates or structurally related intermediates generated in independent ways. However, the absorption spectra of bifunctional radical cations,[2–5] which are generated in a variety of electron-transfer reactions, often do not correspond to those associated with either of the component functionalities. In most of these cases, the spectra have dual characteristics that correspond to both the radical and the cation subunits. There is great interest in radical cations that have mixed spectral properties of this type because this phenomenon might lead to new functions of the radical cations.[6]

[a] Prof. Dr. H. Ikeda, Prof. Dr. K. Mizuno
Department of Applied Chemistry
Graduate School of Engineering
Osaka Prefecture University
Sakai, Osaka 599-8531 (Japan)
Fax: (+81) 72-254-9289
E-mail: ikeda@chem.osakafu-u.ac.jp

[b] Dr. Y. Hoshi, Dr. H. Namai, Dr. F. Tanaka
Department of Chemistry Graduate School of Science
Tohoku University (TU), Sendai, Miyagi 980-8578 (Japan)

[c] Prof. Dr. J. L. Goodman
Department of Chemistry, University of Rochester
Rochester, New York 14627 (USA)

Supporting information for this article is available on the WWW under http://www.chemeurj.org/ or from the author. It contains information on the general methods used and descriptions of the preparation of **1**, **11**, and **12**.

We have previously reported that the PET-induced degenerate Cope rearrangement of 2,5-diphenyl-3,3,4,4-tetradeuterio-1,5-hexadiene ([D_4]**1d**) occurs by a radical-cation cyclization (RCCY)–diradical cleavage (DRCL) mechanism (Scheme 1).[7] The key intermediate in this pathway, the 1,4-

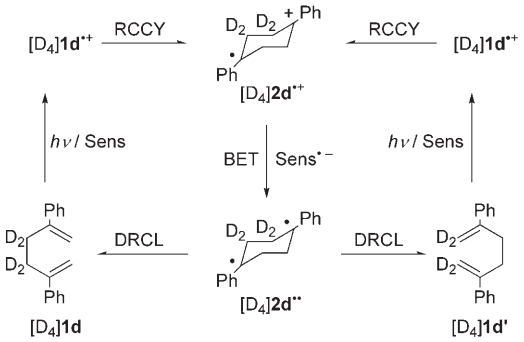

Scheme 1. PET-induced degenerate Cope rearrangement of 2,5-diphenyl-3,3,4,4-tetradeuterio-1,5-hexadiene ([D_4]**1d**). Sens = sensitizer; RCCY = radical cation cyclization; DRCL = diradical cleavage; BET = back electron transfer.

diphenylcyclohexane-1,4-diyl radical cation (**2d**$^{\bullet+}$), was observed spectroscopically. By using nanosecond-resolved laser flash photolysis (LFP) and the *N*-methylquinolinium tetrafluoroborate ($NMQ^+BF_4^-$)/biphenyl (BP) co-sensitization technique, the absorption maximum (λ_{ob}) of **2d**$^{\bullet+}$ was observed at 476 nm[8] in dichloromethane (Figure 1a). Interest-

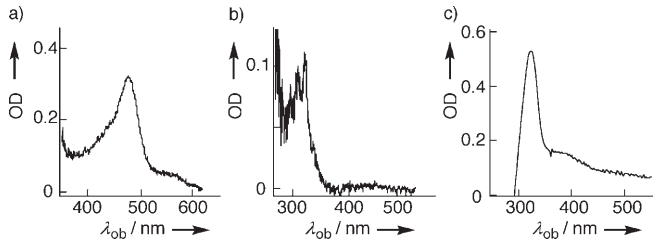

Figure 1. Comparison of the absorption spectra of a) **2d**$^{\bullet+}$ in CH_2Cl_2 at ambient temperatures, b) **3d**$^{\bullet}$ in cyclohexane at ambient temperature, and c) **3d**$^+$ in HSO_3F at −78 °C.

ingly, the λ_{ob} of **2d**$^{\bullet+}$ appears at an unusually long wavelength in comparison with those of its chromophoric components, the cumyl radical (**3d**$^{\bullet}$, λ_{ob} = 322 nm in cyclohexane, Figure 1b)[9,10] and the cumyl cation (**3d**$^+$, λ_{ob} = 322 nm in HSO_3F, Figure 1c).[11,12]

Williams reported earlier that the parent cyclohexane-1,4-diyl radical cation (**4**$^{\bullet+}$) in its chair conformation has a λ_{ob} at

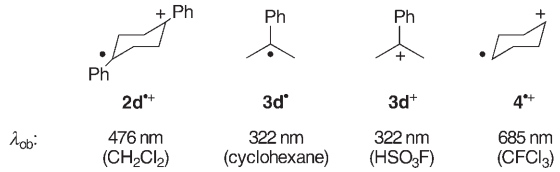

685 nm in $CFCl_4$.[13] Moreover, he proposed that a through-bond (TB) interaction takes place in **4**$^{\bullet+}$ and that the observed absorption band corresponds to a singly occupied molecular orbital (SOMO)→lowest unoccupied molecular orbital (LUMO) transition. At first sight, it might appear that a similar TB interaction could be occurring in **2d**$^{\bullet+}$ and that a SOMO→LUMO transition might account for the absorption band at 476 nm for this intermediate. However, the dramatically shorter wavelength maximum, relative to that of nonphenyl-substituted **4**$^{\bullet+}$, strongly indicates that another interaction and transition are involved in **2d**$^{\bullet+}$.

In a similar manner, electronic coupling has been suggested to explain the λ_{ob} of the chair and boat conformations of the 1,4-bis(4-methoxyphenyl)-2,3-dimethylcyclohexane-1,4-diyl radical cations (*aaC*-**5a**$^{\bullet+}$ and *n,cB*-**5a**$^{\bullet+}$, Scheme 2a)[2]

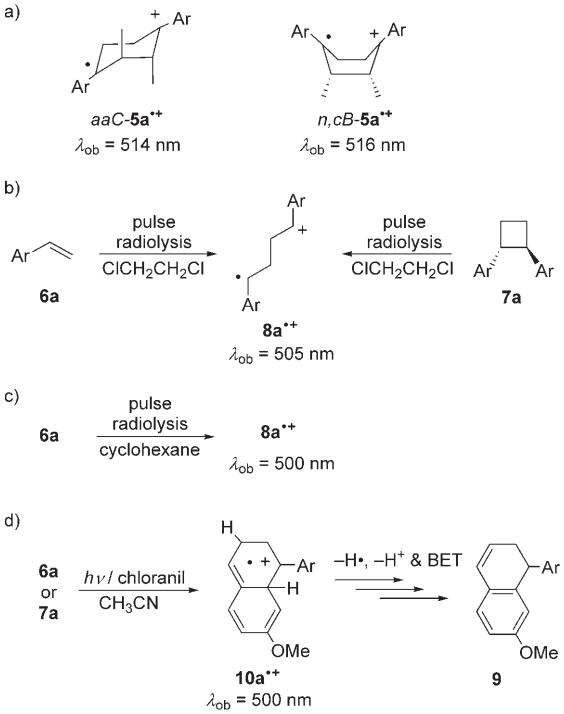

Scheme 2. **a**: Ar = 4-$CH_3OC_6H_4$.

and the 1,4-diarylbutane-1,4-diyl radical cation (**8**$^{\bullet+}$, Scheme 2b).[3,4] Takamuku et al. observed an unusually long wavelength absorption band at λ_{ob} = 505 nm when 4-methoxystyrene (**6a**) and 1,2-bis(4-methoxyphenyl)cyclobutane (**7a**) were independently subjected to pulse radiolysis in 1,2-dichloroethane.[3] These workers assigned the band to **8a**$^{\bullet+}$ and proposed the possibility that an electronic interaction was taking place. Steenken et al. also observed an abnormally long wavelength absorption band at 500 nm for **8a**$^{\bullet+}$ (Scheme 2c) and its aryl analogues, generated by pulse radiolysis of **6a**.[4] In addition, a transient with a λ_{ob} = 500 nm was observed to form in PET reactions of **6a** or **7a** (Scheme 2d).[5] Interestingly, this band was assigned to the cyclic hexatriene radical cation derivative **10a**$^{\bullet+}$, formed by intramolecular cycloaddition of **8a**$^{\bullet+}$, owing to the fact that

dihydronaphthalene derivative **9** is the product of this reaction.

The confusion and controversy surrounding the assignment of transients to long wavelength absorption bands and the characterization of electronic structures of 1,4-radical cations, especially the aryl-substituted derivatives, led us to carry out further investigations on the 1,4-diphenylcyclohexane-1,4-diyl radical cation. To gain further insight into the electronic interactions taking place in this system and the electronic transition responsible for the absorption band, we examined the effects of substituents on λ_{ob} for several *p*-phenyl-substituted derivatives of $\mathbf{2}^{\bullet+}$, along with those of the cumyl radical $\mathbf{3}^{\bullet}$ and cumyl cation $\mathbf{3}^{+}$. These transients were generated from 2,5-diaryl-1,5-hexadienes (**1**), α,α′-azocumene derivatives (**11**), and α-methylstyrene derivatives (**12**), respectively (Scheme 3). In addition, we performed theoretical calculations on these species by using density functional theory (DFT) and time-dependent (TD) DFT methods. We observed that *p*-phenyl substitution in $\mathbf{2d}^{\bullet+}$ with CH_3O, CH_3, F, Cl, and Br groups caused an increasingly large redshift of λ_{ob}. A Hammett plot of the relative transition energies, $\Delta E_{ob}(\mathbf{2}^{\bullet+})$, versus σ^{+} gave two intersecting straight lines with negative and positive ρ values. Similar substituent effects were observed for ΔE_{ob} of $\mathbf{3}^{+}$. Interestingly, a comparison of the ρ values for $\mathbf{2}^{\bullet+}$ and $\mathbf{3}^{+}$ indicated that the effects of substituents on $\Delta E_{ob}(\mathbf{2}^{\bullet+})$ are only half of those on $\Delta E_{ob}(\mathbf{3}^{+})$. The observed redshift and smaller effects of substituents for $\mathbf{2}^{\bullet+}$ are successfully reproduced in the results of the TD-DFT calculations carried out at the (U)B3LYP/cc-pVDZ level. A detailed analysis of the molecular orbitals (MOs), computed by DFT calculations, and a consideration of orbital interaction theory leads to the reasonable proposal that through-space (TS) and TB interactions take place in the chair conformation of $\mathbf{2d}^{\bullet+}$ and that a SOMO-3→SOMO transition is associated with the absorption band at 476 nm.[14] Below, we present detailed results of this study and a discussion of the mechanistic features involved in TS and TB electronic couplings in $\mathbf{2d}^{\bullet+}$.

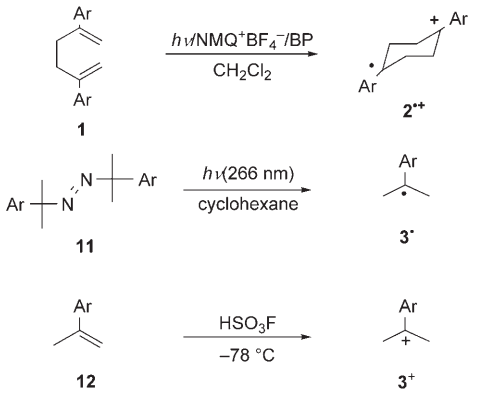

Scheme 3. Generation of *p*-phenyl-substituted derivatives of $\mathbf{2}^{\bullet+}$, the cumyl radical $\mathbf{3}^{\bullet}$, and the cumyl cation $\mathbf{3}^{+}$ from 2,5-diaryl-1,5-hexadienes (**1**), α,α′-azocumene derivatives (**11**), and α-methylstyrene derivatives (**12**), respectively. Ar = 4-XC_6H_4; X = CH_3O, CH_3, F, H, Cl, Br, and I for **a**, **b**, **c**, **d**, **e**, **f**, and **g**, respectively.

Results

Syntheses of 1, 11, and 12: The syntheses of the 4-methoxyphenyl, 4-methylphenyl, phenyl, and 4-chlorophenyl derivatives of 2,5-diaryl-1,5-hexadiene **1** have been described previously.[7a] The 4-fluorophenyl, 4-bromophenyl, and 4-iodophenyl derivatives (**1c**, **1f**, and **1g**) were prepared by Wittig methylenation of the corresponding 1,4-diaryl-1,4-butadiones. The four α,α′-azocumene derivatives **11b–e** were prepared from the corresponding amines (**13**) through sulfamides (**14**) by a slight modification of the procedures described by Timberlake and co-workers[15,16] (Scheme 4). α-Methylstyrenes **12a–g** were generated by Wittig olefination of the corresponding acetophenones.

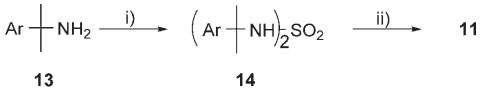

Scheme 4. Preparation of α,α′-azocumene derivatives **11b–e** from the corresponding amines **13**. Reagents: i) SO_2Cl_2, Et_3N, CH_2Cl_2; ii) NaH, *t*BuOCl, THF. Ar = 4-XC_6H_4; X = CH_3, F, H, and Cl for **b**, **c**, **d**, and **e**, respectively.

Electron-donating properties of 1: The respective half-wave oxidation potentials ($E^{ox}_{1/2}$) determined for **1a–g** are +1.27, +1.54, +1.92, +1.68, +1.71, +1.76, and +1.62 V versus SCE in acetonitrile. These values indicate that exothermic hole transfer from $BP^{\bullet+}$, which is generated by electron-transfer from BP ($E^{ox}_{1/2}$ = +1.90 V) to the excited state of $NMQ^{+}BF_4^{-}$, to these dienes will take place to generate the corresponding radical cations $\mathbf{1}^{\bullet+}$ that are the precursors of the 1,4-diarylcyclohexane-1,4-diyl radical cations $\mathbf{2}^{\bullet+}$.

Effects of substituents on λ_{ob} for $\mathbf{2}^{\bullet+}$: The absorption spectra of $\mathbf{2a–g}^{\bullet+}$ were recorded by independently subjecting solutions of the precursor dienes **1a–g** in dichloromethane to nanosecond-resolved LFP (308 nm) by using the $NMQ^{+}BF_4^{-}$/BP co-sensitization technique. As was previously observed for the diphenyl derivative $\mathbf{2d}^{\bullet+}$ (λ_{ob} = 476 nm), $\mathbf{2a–c}^{\bullet+}$ and $\mathbf{2e–g}^{\bullet+}$ have λ_{ob} values of 522, 496, 473, 499, 509, and 539 nm, respectively.[17] Therefore, the incorporation of substituents at the *para* positions of the phenyl groups results in a redshift of λ_{ob}. The lone exception to this is the fluorine-substituted derivative $\mathbf{2c}^{\bullet+}$. The λ_{ob} values observed for $\mathbf{2}^{\bullet+}$ are listed in Table 1, together with the relative transition energies (ΔE_{ob}) based on the absolute transition energies (hc/λ_{ob}) of the phenyl derivative $\mathbf{2d}^{\bullet+}$ [Eq. (1)].

$$\Delta E_{ob} = hc\left[\frac{1}{\lambda_{ob}} - \frac{1}{\lambda_{ob}(\text{phenyl})}\right] \quad (1)$$

As the plot shown in Figure 2 demonstrates, an excellent correlation exists between $\Delta E_{ob}(\mathbf{2}^{\bullet+})$ for $\mathbf{2a–f}^{\bullet+}$ and Creary's substituent constants, $\sigma_C^{\bullet}$.[18] The linear relationship between

Table 1. Substituent constants ($\sigma_c^{\cdot}$ and σ^+), absorption maxima (λ_{ob}), and relative transition energies (ΔE_{ob}) of $\mathbf{2}^{\cdot+}$, $\mathbf{3}^{\cdot}$, and $\mathbf{3}^+$.

			$\mathbf{2}^{\cdot+}$		$\mathbf{3}^{\cdot}$		$\mathbf{3}^+$	
X	$\sigma_C^{\cdot}$[a]	σ^+	λ_{ob}[b] [nm]	ΔE_{ob} [eV]	λ_{ob}[c] [nm]	ΔE_{ob} [eV]	λ_{ob}[d] [nm]	ΔE_{ob} [eV]
a: CH_3O	0.24	−0.78	522	−0.230	[e]		362[f]	−0.425
b: CH_3	0.11	−0.31	496	−0.105	322	0	338[g]	−0.182
c: F	−0.08	−0.07	473	0.017	[h]		324	−0.024
d: H	0	0	476[i]	0	322[j]	0	322[k]	0
e: Cl	0.12	0.11	499	−0.120	318	0.048	348[l]	−0.288
f: Br	0.14	0.15	509	−0.169			364	−0.444
g: I	[m]	0.14	539	−0.304			422	−0.912

[a] See ref. [18]. [b] In CH_2Cl_2. [c] In cyclohexane. [d] In HSO_3F. [e] The value of $\lambda_{ob}(\mathbf{3a}^{\cdot})$ was reported to be 290 nm (NaY) in ref. [19]. [f] See ref. [20]. [g] See ref. [21]. [h] Not detectable. [i] See ref. [8]. [j] See ref. [9]. [k] See ref. [11]. [l] See ref. [22]. [m] Not available.

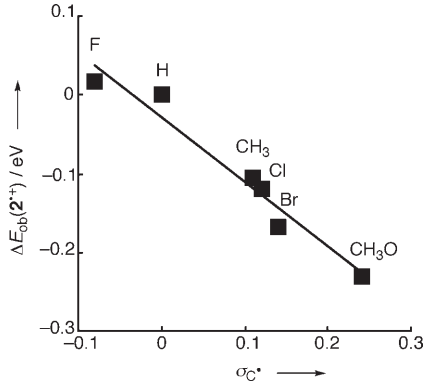

Figure 2. Correlation between $\Delta E_{ob}(\mathbf{2}^{\cdot+})$ and $\sigma_C^{\cdot}$.

$\Delta E_{ob}(\mathbf{2}^{\cdot+})$ and $\sigma_C^{\cdot}$ is expressed in Equation (2):[23]

$$\Delta E_{ob}(\mathbf{2}^{\cdot+}) \approx -0.82\sigma_C^{\cdot} \text{ for } \mathbf{2a\text{-}f}^{\cdot+} \quad (2)$$

A plot of ΔE_{ob} for $\mathbf{2a\text{–}f}^{\cdot+}$ versus the substituent constant σ^+ consists of two intersecting lines (Figure 3).[24] The finding that $\Delta E_{ob}(\mathbf{2}^{\cdot+})$ correlates with both the $\sigma_C^{\cdot}$ and σ^+ parameters is consistent with the dual radical and cationic nature of $\mathbf{2}^{\cdot+}$. The two linear relationships between $\Delta E_{ob}(\mathbf{2}^{\cdot+})$ and σ^+ are given by Equation (3) and (4):[23]

$$\Delta E_{ob}(\mathbf{2}^{\cdot+}) \approx 0.32\sigma^+ \text{ for } \mathbf{2a\text{-}d}^{\cdot+} \quad (3)$$

$$\Delta E_{ob}(\mathbf{2}^{\cdot+}) \approx -1.12\sigma^+ \text{ for } \mathbf{2d\text{-}f}^{\cdot+} \quad (4)$$

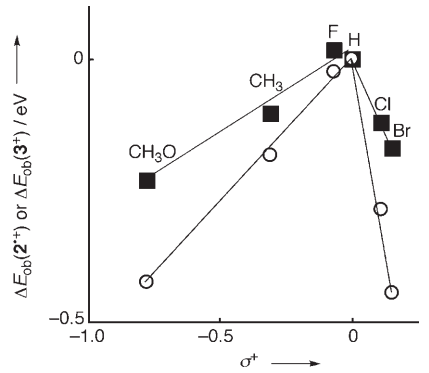

Figure 3. Correlation between experimental $\Delta E_{ob}(\mathbf{2}^{\cdot+})$ (squares) or $\Delta E_{ob}(\mathbf{3}^+)$ (circles) and σ^+.

The correlation between ΔE_{ob} for $\mathbf{2a\text{–}d}^{\cdot+}$ and σ^+ is associated with a ρ value of 0.32. In contrast, a negative ρ value of −1.12 is found for the correlation between $\mathbf{2d\text{–}f}^{\cdot+}$ and σ^+.[24] The dual phase nature of substituent effects on the transition energies was also observed in our recent work with geminally diaryl-substituted trimethylenemethane (TMM)-type radical cations and diarylethyl cations.[25] In these cases, Cl and Br substituents acted as electron-donating groups in governing the electronic transitions.

Effects of substituents on the λ_{ob} for $\mathbf{3}^{\cdot}$ and $\mathbf{3}^+$: To gain information about how the effects of substituents on λ_{ob} for $\mathbf{2}^{\cdot+}$ observed reflect the odd nature of the electron- and charge-partitioning in the component cumyl moieties, the cumyl radical $\mathbf{3}^{\cdot}$ and cation $\mathbf{3}^+$ were generated independently from **11** and **12**, respectively (Scheme 3). Azocumenes **11b–e** were subjected to LFP (266 nm) under direct irradiation conditionsin degassed cyclohexane at ambient temperature.[10b] Although no clear transient absorption was detected when **11c** was irradiated, LFP of **11b**, **11d**, and **11e** generated transients with λ_{ob} at 322, 322,[9] and 318 nm, respectively, which were assigned to $\mathbf{3b}^{\cdot}$, $\mathbf{3d}^{\cdot}$, and $\mathbf{3e}^{\cdot}$, respectively (Table 1). Clearly, no significant effects of substituents on λ_{ob} for $\mathbf{3}^{\cdot}$ were observed.

In contrast, substituents have a significant effect on the λ_{ob} of $\mathbf{3}^+$. These transients were generated from **12a–g** in HSO_3F at −78 °C by using a slight modification of the procedure described by Sekuur and Kranenburg.[12a] The λ_{ob} values for the cumyl cations $\mathbf{3a\text{–}g}^+$ formed in this manner are listed in Table 1. Cations $\mathbf{3a\text{–}g}^+$ exhibited intense absorption bands with the λ_{ob} at 362,[20] 338,[21] 324, 322,[11] 348,[22] 364, and 422 nm, respectively. As expected, substituents at the *para* positions of the phenyl groups in these transients give rise to redshifts of the λ_{ob}. The most significant observation is that the effects of substituent on λ_{ob} for $\mathbf{3a\text{–}f}^+$ are much greater than those on the absorption maxima of $\mathbf{2a\text{–}f}^{\cdot+}$. This result is best seen by viewing the plot of $\Delta E_{ob}(\mathbf{3}^+)$, based on $hc/\lambda_{ob}(\mathbf{3d}^+)$, versus σ^+, displayed in Figure 3. As observed for $\mathbf{2a\text{–}f}^{\cdot+}$, the Hammett plot for $\mathbf{3a\text{–}f}^+$ is comprised of two intersecting straight lines, expressed by Equations (5) and (6),[23] which correspond to ρ values of 0.55 and −2.89, respectively.

$$\Delta E_{ob}(\mathbf{3}^{+}) \approx 0.55\sigma^{+} \text{ for } \mathbf{3a}\text{-}\mathbf{d}^{+} \quad (5)$$

$$\Delta E_{ob}(\mathbf{3}^{+}) \approx -2.89\sigma^{+} \text{ for } \mathbf{3d}\text{-}\mathbf{f}^{+} \quad (6)$$

The differences between the magnitudes of the effects of substituents on λ_{ob} for $\mathbf{2}^{\bullet+}$ and $\mathbf{3}^{+}$ were evaluated by using Equations (7) and (8). The $\rho(\mathbf{2}^{\bullet+})/\rho(\mathbf{3}^{+})$ ratio is approximately 0.6 when comparing $\mathbf{2a}$–$\mathbf{d}^{\bullet+}$ and $\mathbf{3a}$–$\mathbf{d}^{+}$ and 0.4 when comparing $\mathbf{2d}$–$\mathbf{f}^{\bullet+}$ and $\mathbf{3d}$–$\mathbf{f}^{+}$. These findings indicate that the substituent effects on the electronic transition energies of $\mathbf{2}^{\bullet+}$ are reduced by approximately half compared with those on the transition energies of $\mathbf{3}^{+}$ in both the $\sigma^{+}<0$ and $\sigma^{+}>0$ regions.

$$\frac{\rho(\mathbf{2}^{\bullet+})}{\rho(\mathbf{3}^{+})} \approx \frac{\Delta E_{ob}(\mathbf{2}^{\bullet+})}{\Delta E_{ob}(\mathbf{3}^{+})} = 0.6 \text{ for } \mathbf{2a}\text{-}\mathbf{d}^{\bullet+} \text{ and } \mathbf{3a}\text{-}\mathbf{d}^{+} \quad (7)$$

$$\frac{\rho(\mathbf{2}^{\bullet+})}{\rho(\mathbf{3}^{+})} \approx \frac{\Delta E_{ob}(\mathbf{2}^{\bullet+})}{\Delta E_{ob}(\mathbf{3}^{+})} = 0.4 \text{ for } \mathbf{2d}\text{-}\mathbf{f}^{\bullet+} \text{ and } \mathbf{3d}\text{-}\mathbf{f}^{+} \quad (8)$$

Discussion

The explanation for the long wavelength absorption band of the parent cyclohexane-1,4-diyl radical cation $\mathbf{4}^{\bullet+}$ based on a TB interaction and SOMO→LUMO transition proposed by Williams[13] cannot easily be applied to the long wavelength absorption band of $\mathbf{2d}^{\bullet+}$. In fact, phenyl substitution of this radical cation (as in $\mathbf{2d}^{\bullet+}$) caused the λ_{ob} to shift to shorter wavelengths in spite of the extension of the conjugate system. Thus, another interaction and/or electronic transition must be taking place in $\mathbf{2d}^{\bullet+}$. We believe that the key to the unusually large wavelength shift of λ_{ob} for $\mathbf{2d}^{\bullet+}$ lies in orbital interactions that take place between the cumyl radical and the cumyl cation components.

DFT and TD-DFT calculations on $\mathbf{2}^{\bullet+}$ and $\mathbf{3}^{+}$: To gain an insight into the factors governing the electronic transitions in $\mathbf{2d}^{\bullet+}$, DFT and TD-DFT calculations were carried out. The results show that $\mathbf{2d}^{\bullet+}$ and $\mathbf{3d}^{+}$, as well as the *para*-substituted counterparts $\mathbf{2a}$–$\mathbf{f}^{\bullet+}$ and $\mathbf{3a}$–$\mathbf{f}^{+}$, have typical chair and planar conformations, respectively, at the (U)B3LYP/cc-pVDZ level of theory (Figure 4).[14]

The electronic transition wavelengths (λ_{cal}) and oscillator strengths (f) in the optimized structures of $\mathbf{2a}$–$\mathbf{f}^{\bullet+}$ and $\mathbf{3a}$–$\mathbf{f}^{+}$ were calculated by using TD-(U)B3LYP/cc-pVDZ, as shown in Figure 5 and Table 2. The TD-DFT calculations successfully reproduced the absorption bands observed in the visible region for $\mathbf{2}^{\bullet+}$ and in the UV region for $\mathbf{3}^{+}$. The calculations suggested that the electronic transitions of $\mathbf{2}^{\bullet+}$ and $\mathbf{3}^{+}$ correspond to a SOMO-X→SOMO ($X=1$ for $\mathbf{2a}^{\bullet+}$, $\mathbf{2c}^{\bullet+}$, $\mathbf{2e}^{\bullet+}$, and $\mathbf{2f}^{\bullet+}$ and $X=3$ for $\mathbf{2b}^{\bullet+}$ and $\mathbf{2d}^{\bullet+}$) and a HOMO-X→LUMO transition ($X=1$ for $\mathbf{3a}^{+}$, $\mathbf{3c}^{+}$, $\mathbf{3e}^{+}$, and $\mathbf{3f}^{+}$ and $X=0$ for $\mathbf{3b}^{+}$ and $\mathbf{3d}^{+}$). Hammett plots of the calculated relative transition energies of $\mathbf{2}^{\bullet+}$ and $\mathbf{3}^{+}$ versus σ^{+} are shown in Figure 6. Excellent correlations are seen in the plots of the data for both $\mathbf{2}^{\bullet+}$ and $\mathbf{3}^{+}$, which consist of two intersecting straight lines represented by Equations (9)–(12):

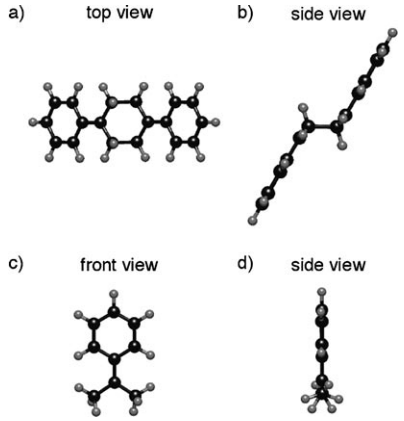

Figure 4. Optimized molecular geometries of $\mathbf{2d}^{\bullet+}$ obtained by using UB3LYP/cc-pVDZ, a) top and b) side views, and of $\mathbf{3d}^{+}$ obtained by using B3LYP/cc-pVDZ, c) front and d) side views.

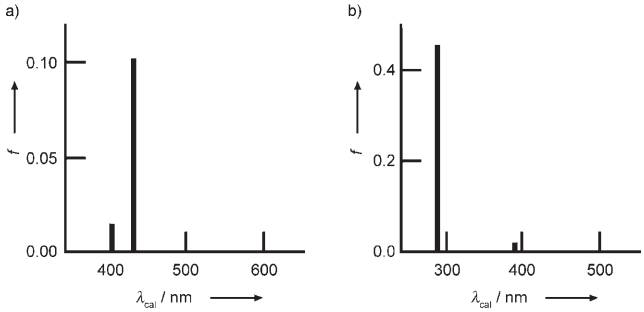

Figure 5. Electronic transitions of a) $\mathbf{2d}^{\bullet+}$ and b) $\mathbf{3d}^{+}$ calculated by using TD-(U)B3LYP/cc-pVDZ.

Table 2. Substituent constants (σ^{+}), calculated electronic transition wavelengths (λ_{cal}), oscillator strengths (f), and relative transition energies (ΔE_{cal}) for $\mathbf{2}^{\bullet+}$ and $\mathbf{3}^{+}$.

		$\mathbf{2}^{\bullet+}$				$\mathbf{3}^{+}$		
X	σ^{+}	λ_{cal}[a] [nm]	f	ΔE_{cal} [eV]	λ_{cal}[a] [nm]	f	ΔE_{cal} [eV]	
a: CH_3O	−0.78	492	0.14	−0.355	330	0.61	−0.551	
b: CH_3	−0.31	451	0.12	−0.129	303	0.58	−0.209	
c: F	−0.08	441	0.10	−0.067	292	0.49	−0.066	
d: H	0.00	431	0.10	0.00	288	0.45	0.00	
e: Cl	0.12	482	0.12	−0.302	325	0.56	−0.491	
f: Br	0.14	510	0.11	−0.446	354	0.52	−0.801	

[a] Calculated at the UB3LYP/cc-PVDZ level of theory.

$$\Delta E_{cal}(\mathbf{2}^{\bullet+}) \approx 0.43\sigma^{+} \text{ for } \mathbf{2a}\text{-}\mathbf{d}^{\bullet+} \quad (9)$$

$$\Delta E_{cal}(\mathbf{2}^{\bullet+}) \approx -2.93\sigma^{+} \text{ for } \mathbf{2d}\text{-}\mathbf{f}^{\bullet+} \quad (10)$$

$$\Delta E_{cal}(\mathbf{3}^{+}) \approx 0.70\sigma^{+} \text{ for } \mathbf{3a}\text{-}\mathbf{d}^{+} \quad (11)$$

$$\Delta E_{cal}(\mathbf{3}^{+}) \approx -5.16\sigma^{+} \text{ for } \mathbf{3d}\text{-}\mathbf{f}^{+} \quad (12)$$

These plots and equations closely match those obtained

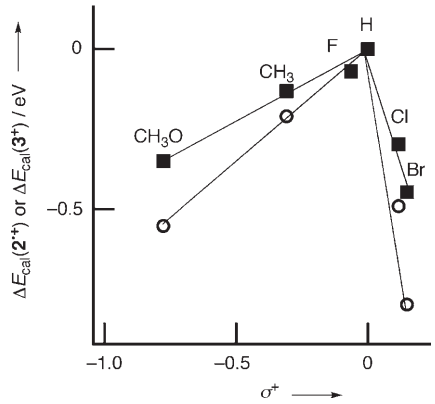

Figure 6. Correlation between computed $\Delta E_{cal}(\mathbf{2}^{\bullet+}$; ■) or $\Delta E_{cal}(\mathbf{3}^{+}$; ○) and σ^{+}.

from the experimental data (Figure 3). Furthermore, the results of the TD-DFT calculations also predict that the magnitude of the substituent effects in $\mathbf{2}^{\bullet+}$ are about half of those in $\mathbf{3}^{+}$ [Eqs (7) and (8)]. The ratio of $\rho(\mathbf{2}^{\bullet+})/\rho(\mathbf{3}^{+})$, obtained as the ratio of $\Delta E_{cal}(\mathbf{2}^{\bullet+})/\Delta E_{cal}(\mathbf{3}^{+})$, is approximately 0.6 for $\mathbf{2}^{\bullet+}$ and $\mathbf{3}^{+}$ [Eqs (13) and (14)]. These findings indicate that the calculations at the (U)B3LYP/cc-pVDZ level of theory are good enough to accurately describe the electronic states of the radical cation and cation systems.

$$\frac{\rho(\mathbf{2}^{\bullet+})}{\rho(\mathbf{3}^{+})} \approx \frac{\Delta E_{cal}(\mathbf{2}^{\bullet+})}{\Delta E_{cal}(\mathbf{3}^{+})} = 0.6 \text{ for } \mathbf{2a\text{-}d}^{\bullet+} \text{ and } \mathbf{3a\text{-}d}^{+} \quad (13)$$

$$\frac{\rho(\mathbf{2}^{\bullet+})}{\rho(\mathbf{3}^{+})} \approx \frac{\Delta E_{cal}(\mathbf{2}^{\bullet+})}{\Delta E_{cal}(\mathbf{3}^{+})} = 0.6 \text{ for } \mathbf{2d\text{-}f}^{\bullet+} \text{ and } \mathbf{3d\text{-}f}^{+} \quad (14)$$

MO diagram of $\mathbf{2d}^{\bullet+}$: To elucidate the cause of the redshift of the absorption band, we analyzed the MOs of $\mathbf{2d}^{\bullet+}$ in detail. A plausible explanation for the computed MOs of $\mathbf{2d}^{\bullet+}$ arises by using two sets of MOs for $\mathbf{3d}^{+}$ calculated with B3LYP/cc-pVDZ and a C–C σ bond for the cyclohexane skeleton (Figure 7). Note that the MOs of $\mathbf{3d}^{\bullet}$ are replaced by those of $\mathbf{3d}^{+}$ for simplicity. In the optimized chair conformation of $\mathbf{2d}^{\bullet+}$, the cumyl radical and the cumyl cation components are sufficiently close (a C–C bond length between the two benzyl carbon atoms of ca. 2.9 Å) to enable TS electronic coupling with each other. The TS interaction is less efficient than the TB interaction (see below), but cannot be omitted because an antiperiplanar approach of the cumyl cation and the cumyl radical resulted in a small change in the MOs in a preliminary calculation. For the TS interaction, φ_1 with bonding character and φ_2 with antibonding character are composed of two χ_1 MOs of $\mathbf{3d}^{+}$ (or $\mathbf{3d}^{\bullet}$). Similarly, φ_5 with bonding character and φ_6 with antibonding character are given by two χ_3 MOs. Note that the two p orbitals at the benzylic position of $\mathbf{3d}^{\bullet}$ and $\mathbf{3d}^{+}$ interact with each other owing to the restricted nature of the chair conformation. The TS interaction between two χ_2 MOs can be omitted because the orbital coefficients at the benzylic carbon atoms are negligible. Furthermore, in this system electronic coupling between the benzyl radical and the benzyl cation components through two σ bonds of the cyclohexane skeleton (the so-called TB interaction) plays a crucial role. Because of the orbital symmetry of the two benzylic positions, φ_1

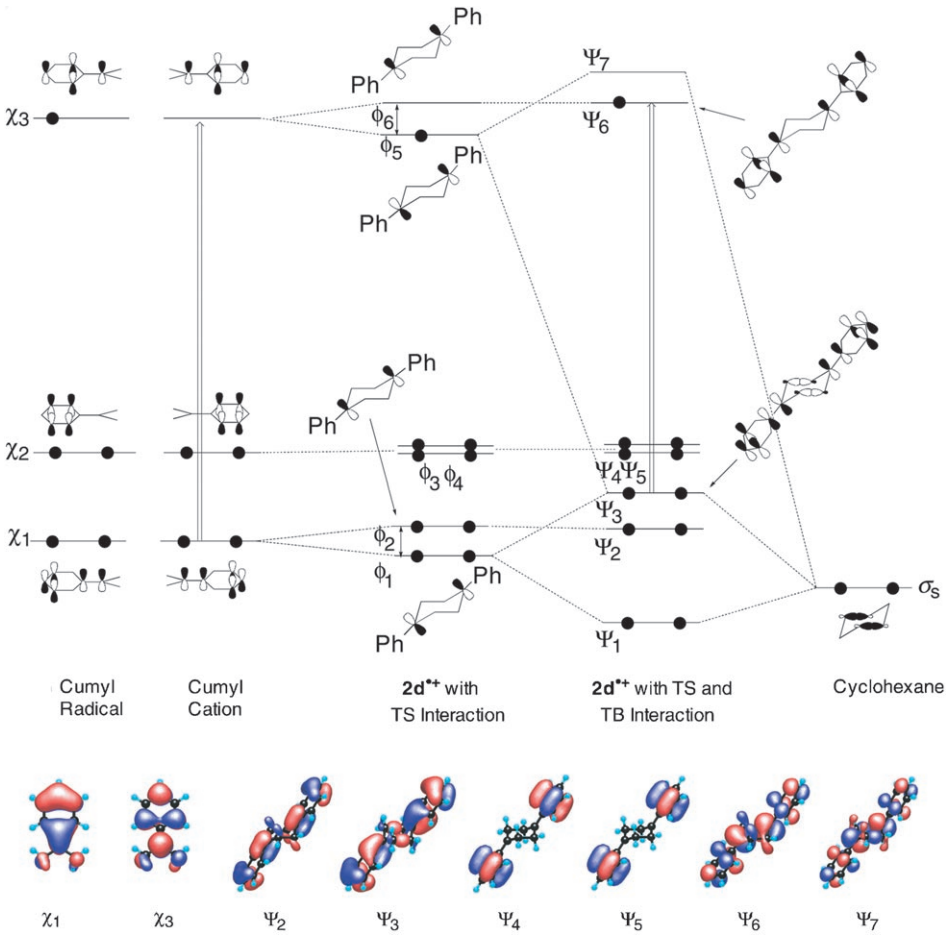

Figure 7. Conceptual representation that shows the TS and TB interactions in $\mathbf{2d}^{\bullet+}$ and some important MOs calculated by using (U)B3LYP/cc-pVDZ.

and φ_5 interact with σ_s, but φ_2 and φ_6 do not. As a result, Ψ_1 with a bonding character and Ψ_3 and Ψ_7 with an antibonding character are produced. MOs of φ_3 and φ_4 do not interact with σ_s for the same reason as described above for χ_2.

The computed MOs, shown in Figure 7, provide strong support for an interpretation of the electronic transition properties of $\mathbf{2d}^{\bullet+}$ based on a combination of TS and TB orbital interactions. Note that both of these types of interactions cause a large rise in the Ψ_3(SOMO-3) level compared with the χ_1(HOMO-1) level, whereas the TS interaction alone causes a slight rise in the Ψ_6(SOMO) level compared with the χ_3(LUMO) level. In this sense, the TB interaction is more dominant than the TS interaction. As a result, the energy gap between Ψ_3 and Ψ_6 becomes smaller than that between χ_1 and χ_3 which govern the respective electronic transitions in $\mathbf{2d}^{\bullet+}$ and $\mathbf{3d}^{+}$. Therefore, the surprising red-shift of the absorption band of $\mathbf{2d}^{\bullet+}$ compared with that of $\mathbf{3d}^{+}$ is in reasonable accord with these considerations.

Note that the orbital distributions of the cumyl subunit of Ψ_3 and Ψ_6 closely resemble those of χ_1 and χ_3, respectively (Figure 7). This finding strongly suggests that the absorption band at 476 nm for $\mathbf{2d}^{\bullet+}$ and the absorption band at 322 nm for $\mathbf{3d}^{+}$ essentially correspond to the same type of electronic transition. The former is not as a result of the destruction of forbidden transitions of the benzyl or cumyl radical skeletons, which are known to appear weakly at around 450 to 500 nm.

Theory for orbital interactions in $\mathbf{2d}^{\bullet+}$: Because the electronic transitions associated with the major absorption bands of $\mathbf{2d}^{\bullet+}$ and $\mathbf{3d}^{+}$ essentially take place between the same types of MOs, one would expect that the effect of substituents on these electronic transitions should be of the same magnitude in both systems. However, the experimental results and TD-DFT calculations both suggest that the magnitude of the substituent effects on the transition energies of $\mathbf{2}^{\bullet+}$ should be about half of those on the transition energies of $\mathbf{3}^{+}$. To reconcile this difference, substitution-induced changes in the energies of the MOs were evaluated by using orbital interaction theory and the simple Hückel method.[26] The energy (E) of the Ψ_3(SOMO-3) of $\mathbf{2d}^{\bullet+}$ is represented by Equation (15), in which e_A, e_B, and h_{AB} are the energies of φ_1, σ_s, and the resonance integral between φ_1 and σ_s, respectively (Figure 8). Accordingly, the energies $E+D$ of the corresponding derivatives $\mathbf{2a}$–$\mathbf{c}^{\bullet+}$ and $\mathbf{2e}$–$\mathbf{f}^{\bullet+}$ can be represented by Equation (16), in which D is the increment in the energy of Ψ_3(SOMO-3) for $\mathbf{2a}$–$\mathbf{c}^{\bullet+}$ and $\mathbf{2e}$-$\mathbf{f}^{\bullet+}$ when an electron-donating group perturbs the MOs, χ_1, of the cumyl radical $\mathbf{3d}^{\bullet}$ and the cumyl cation $\mathbf{3d}^{+}$ with energy d. Note that although they are generally regarded as electron-withdrawing, Cl and Br are treated as electron-donating groups, which was shown to be the case in our recent work.[25] Therefore, D and d correspond to $\Delta E(\mathbf{2}^{\bullet+})$ and $\Delta E(\mathbf{3}^{+})$, respectively. Note that an increase in the energy of d in χ_1 gives rise to a roughly equal increase in the energy of φ_1 (Figure 8).[27] Therefore the energy gap D is given by Equation (17).

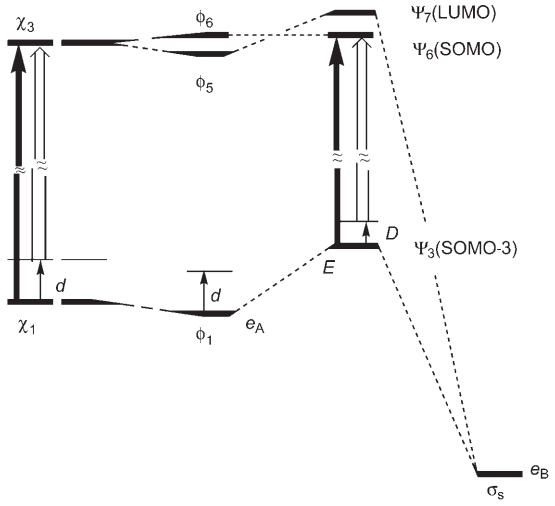

Figure 8. Selected MO diagram that shows the substituent effects in $\mathbf{2}^{\bullet+}$. The symbols e_A, e_B, and E represent the energies of the φ_1, σ_s, and Ψ_3-(SOMO-3) orbitals of $\mathbf{2d}^{\bullet+}$, respectively. d and D represent the increment in the energy of the χ_1 (and φ_1) and Ψ_3(SOMO-3) orbitals of $\mathbf{2a}$–$\mathbf{c}^{\bullet+}$ and $\mathbf{2e}$–$\mathbf{f}^{\bullet+}$, respectively, induced by substitution of an electron-donating group.

$$E = \{e_A + e_B + [(e_A - e_B)^2 + 4h_{AB}^2]^{1/2}\}/2 \quad (15)$$

$$E + D = \{e_A + d + e_B + [(e_A + d - e_B)^2 + 4h_{AB}^2]^{1/2}\}/2 \quad (16)$$

$$D = \{d + [(e_A + d - e_B)^2 + 4h_{AB}^2]^{1/2} - [(e_A - e_B)^2 + 4h_{AB}^2]^{1/2}\}/2 \quad (17)$$

When no TB interaction occurs and no resonance integral between φ_1 and σ_s ($h_{AB}=0$) exists, D is equal to d and a large energy gap ($e_A - e_B \gg 0$) is present. However, D will decrease to $0.5d$ when there is an effective TB interaction with a large h_{AB} and a small $e_A - e_B$. Therefore, the ratio D/d changes from 0.5 to unity, as shown in Equation (18):

$$0.5 < D/d < 1 \quad (18)$$

The experimentally observed relative energy ratios $\Delta E_{ob}(\mathbf{2}^{\bullet+})/\Delta E_{ob}(\mathbf{3}^{+})$ of 0.6 and 0.4 when $\sigma^+ < 0$ and $\sigma^+ > 0$, respectively [Eqs. (7) and (8)], successfully reproduced by TD-DFT calculations, are close to 0.5 [Eqs. (13) and 14)].[28] Thus, TB interactions in $\mathbf{2}^{\bullet+}$ must be near the maximum predicted by orbital interaction theory. In other words, the smaller effect of substituents on the transition energies of $\mathbf{2}^{\bullet+}$ compared with those of $\mathbf{3}^{+}$, in spite of the fact that they correspond to the same types of electronic transitions, strongly suggest that substantial TS and TB interactions exist in $\mathbf{2}^{\bullet+}$.

Conclusion

The results of this work have demonstrated that the effect of substituents on the absorption spectra of $\mathbf{2}^{\bullet+}$ can be ra-

tionalized by considering TS and TB electronic coupling of the cumyl radical and the cumyl cation components. DFT calculations[29] and orbital interaction theoretical considerations suggest that TS and TB interactions are operative in $\mathbf{2d}^{\bullet+}$ and that $\Psi_3(\text{SOMO-3})\rightarrow\Psi_6(\text{SOMO})$ transitions are responsible for the characteristic absorption band in the visible region. Therefore, the observed redshift of the λ_{ob} and the smaller effect of substituents both arise from TS and TB interactions. This investigation has led to the first theoretical explanation of the unusually long wavelength absorption bands observed for aryl-substituted 1,4-radical cations.[30] They are often called distonic radical cations. However, this may be a misleading term because its use sometimes implies the separation of spin and positive charge in a molecule. There is of course no such separation in a delocalized structure that results from orbital interactions.

Although we are reluctant to comment on the controversy that involves the acyclic radical cation $\mathbf{8}^{\bullet+}$ (see the Introduction), the results of our studies suggest that electronic coupling, probably through TS and TB interactions, rather than intramolecular cycloadditions is a more likely explanation of earlier observations. Similar electronic coupling (but probably involving pseudo-π orbitals[31]) can explain the long wavelength absorption band of the 1,3-diarylpropane-1,3-diyl[3a] and 1,3-diarylcyclohexane-1,3-diyl radical cations.[2b] Our results not only provide a meaningful interpretation of the interactions in pure radical cations,[32] but they also give information that assists the design of bifunctional radical cations as part of the development of conceptually new chromophores and fluorophores[6,33] in which orbital interactions take place between small subunits. In particular, we recently found a new and general strategy to observe short-lived biradicals, such as the singlet-excited state of 1,4-diphenylcyclohexane-1,4-diyl ($^1\mathbf{2d}^{\bullet\bullet}$), which is a one-electron reduced species of $\mathbf{2d}^{\bullet+}$ (Scheme 5). Biradical $^1\mathbf{2d}^{\bullet\bullet}$ was observed at $\lambda_{em}=582$ nm as thermoluminescence from the excited state of $^1\mathbf{2d}^{\bullet\bullet}$ ($^1\mathbf{2d}^{\bullet\bullet *}$). This extraordinary long wavelength emission should also be explained by similar significant TS and TB electronic coupling between the two cumyl radical subunits in $^1\mathbf{2d}^{\bullet\bullet *}$.[33]

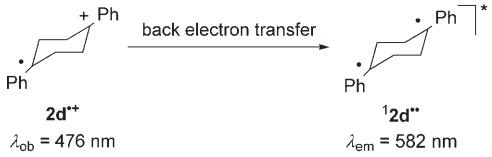

Scheme 5. Generation of the excited singlet biradical $^1\mathbf{2d}^{\bullet\bullet *}$ by back electron transfer to $\mathbf{2d}^{\bullet+}$ in the thermoluminescence experiment.

Experimental Section

Spectroscopic observation of $\mathbf{2}^{\bullet+}$: A solution of **1** (10 mM), $NMQ^+BF_4^-$ (1 mM), and BP (0.4 M) in aerated CH_2Cl_2 (2 mL) in a quartz cell of 1 cm pathlength was irradiated at 308 nm through a focusing lens by using an excimer laser. The beam diameter at the sample was around 10 mm. The values of the absorbance at selected times (170–280, 270–380, and 470–580 ns, and 1.07–1.18, 2.07–2.18, 5.07–5.18, 10.1–10.2, 20.1–20.2, 50.1–50.2, and 100–101 μs) after excitation were monitored by using a Xe arc lamp and spectrophotometer. The data collection time was observed by using an oscilloscope. The delay times of the delay unit were 100, 200, and 400 ns, and 1, 2, 5, 10, 20, 50, and 100 μs. The gate width of the image intensifier was 100 ns. To improve the signal-to-noise ratio, each difference absorption spectrum was the result of averaging data from at least five excitation pulses. The monitoring light was directed onto the sample cell with a fiberglass cable. The transmitted beams were led to an image intensifier coupled to a multichannnel detector controller with a second fiberglass cable. This detector was interfaced with a personal computer that controlled the necessary optical hardware and electronics during data acquisition, processed the data, and presented the data graphically. The wavelengths of the spectrophotometer were calibrated at 360.8, 418.5, and 536.4 nm with holmium oxide. The difference absorption spectra span wavelength ranges of approximately 350 to 630 or 500 to 780 nm. See the Supporting Information for transient absorption spectra of $\mathbf{2}^{\bullet+}$.

Spectroscopic observation of $\mathbf{3}^{\bullet}$: A solution of **11** (3 mM) in cyclohexane (4 mL) in a quartz cell of 1 cm pathlength was saturated with argon, degassed by using several repeated freeze (−196 °C)–pump (10^{-2} Torr)–thaw (ambient temperature) cycles, and then sealed at 10^{-2} Torr. This solution was irradiated at 266 nm through a focusing lens by using a YAG laser at ambient temperature. The beam diameter at the sample was around 5 mm. Data collection was similar to that described for $\mathbf{2}^{\bullet+}$. The difference absorption spectrum spans a wavelength range of approximately 250–530 nm.

Spectroscopic observation of $\mathbf{3}^{+}$: Absorption spectra of $\mathbf{3}^{+}$ were obtained by using a slight modification of the procedure reported by Sekuur and Kranenburg.[12a] A quartz cell that contained HSO_3F (2 mL) was quickly sealed with a rubber septum, saturated with argon by bubbling the gas through the solution, and cooled to −78 °C in a 4×4 cm quartz Dewar flask. A solution of **12** (3–6 mM) in MeOH (5–50 μL) was added to the quartz cell by using a microsyringe. Absorption spectra of $\mathbf{3}^{+}$ were recorded after stirring for 5 min at −78 °C. See the Supporting Information for the transient absorption spectra of $\mathbf{3}^{+}$.

Quantum chemical calculations: DFT and TD-DFT calculations were performed by using the Gaussian 98 package of programs.[34] Figures 4 and 7 were drawn by using WinMOPAC 3.9 software.[35] The cartesian coordinates for the optimized structures of $\mathbf{2d}^{\bullet+}$ are given in the Supporting Information.

Acknowledgements

H.I. and K.M. gratefully acknowledge financial support from a Grant-in-Aid for Scientific Research on Priority Areas (Nos. 14050008 and 17029058 in Area No. 417) and others (Nos. 09740536, 10640507, 122440173, and 19350025) from the Ministry of Education, Culture, Sports, Science, and Technology (MEXT) of Japan. H.I. also thanks Izumi, Iketani, Shorai, and Mazda Science and Technology Foundations for providing financial support for the work. We also thank Professor Emeritus T. Miyashi (TU) and Professor M. Ueda (TU) for their insightful and generous suggestions.

[1] a) J. C. Scaiano, *CRC Handbook of Organic Photochemistry*, CRC, Boca Raton, **1989**; b) L. J. Johnston, N. P. Schepp, "Kinetics and Mechanisms for the Reactions of Alkene Radical Cations" in *Advances in Electron Transfer Chemistry*, *Vol. 5* (Ed.: P. S. Mariano), JAI Press, London, **1996**, pp. 41–102.

[2] a) H. Ikeda, T. Takasaki, Y. Takahashi, A. Konno, M. Matsumoto, Y. Hoshi, T. Aoki, T. Suzuki, J. L. Goodman, T. Miyashi, *J. Org. Chem.* **1999**, *64*, 1640–1649; b) H. Ikeda, Y. Hoshi, T. Miyashi, *Tetrahedron Lett.* **2001**, *42*, 8485–8488.

[3] a) S. Tojo, S. Toki, S. Takamuku, *J. Org. Chem.* **1991**, *56*, 6240–6243; b) S. Tojo, S. Toki, S. Takamuku, *Radiat. Phys. Chem.* **1992**, *40*, 95–99.

[4] O. Brede, F. David, S. Steenken, *J. Chem. Soc., Perkin Trans. 2* **1995**, 23–32.

[5] N. P. Schepp, L. J. Johnston, *J. Am. Chem. Soc.* **1994**, *116*, 6895–6903.

[6] H. Namai, H. Ikeda, Y. Hoshi, N. Kato, Y. Morishita, K. Mizuno, *J. Am. Chem. Soc.* **2007**, *129*, 9032–9036.

[7] a) H. Ikeda, T. Minegishi, H. Abe, A. Konno, J. L. Goodman, T. Miyashi, *J. Am. Chem. Soc.* **1998**, *120*, 87–95; b) H. Ikeda, T. Minegishi, Y. Takahashi, T. Miyashi, *Tetrahedron Lett.* **1996**, *37*, 4377–4380; c) T. Miyashi, H. Ikeda, Y. Takahashi, *Acc. Chem. Res.* **1999**, *32*, 815–824.

[8] The value of 482 nm for the λ_{ob} of $\mathbf{2d}^{\bullet+}$ in dichloromethane, which was reported in ref. [7], was revised to 476 nm after wavelength calibration of the spectrophotometer. See the Experimental Section.

[9] Values for $\lambda_{ob}(\mathbf{3d}^{\bullet})$ of 315 (cyclohexane) and 322 nm (cyclohexane) have been reported in refs. [10a] and [10b], respectively.

[10] a) D. R. Boate, J. C. Scaiano, *Tetrahedron Lett.* **1989**, *30*, 4633–4636; b) T. Sumiyoshi, M. Kamachi, Y. Kuwae, W. Schnabel, *Bull. Chem. Soc. Jpn.* **1987**, *60*, 77–81.

[11] Values for $\lambda_{ob}(\mathbf{3d}^{+})$ of 317 (HSO_3F), 325 (CF_3CH_2OH), and 326 nm (HSO_3F–SbF_3) have been reported in refs. [12a], [12b], and [12c], respectively.

[12] a) T. J. Sekuur, P. Kranenburg, *Spectrochim. Acta, Part A* **1973**, *29*, 803–805; b) R. A. McClelland, C. Chan, F. Cozens, A. Modro, S. Steenken, *Angew. Chem.*, **1991**, *103*, 1389–1391; *Angew. Chem. Int. Ed. Engl.* **1991**, *30*, 1337–1339; c) G. A. Olah, C. U. Pittman, Jr., R. Waack, M. Doran, *J. Am. Chem. Soc.* **1966**, *88*, 1488–1495.

[13] F. Williams, *J. Chem. Soc., Faraday Trans.* **1994**, *90*, 1681–1687.

[14] The chair conformation of $\mathbf{2}^{\bullet+}$ is strongly suggested by the stereochemistry of the PET Cope rearrangements of 3,6-diaryl-2,6-octadienes and 2,5-diaryl-3,4-dimethyl-1,5-hexadienes (see ref. [2a]). As one reviewer suggested, it is important to consider other molecular geometries, especially a twisted boat form. The results of a preliminary calculation suggested the twisted boat conformation of $\mathbf{2}^{\bullet+}$ has a similar, but probably less efficient, orbital interaction. To clarify, we discuss here only the chair form of $\mathbf{2}^{\bullet+}$, which is optimized as the most stable molecular geometry.

[15] J. W. Timberlake, J. Alender, A. W. Garner, M. L. Hodges, C. Ozmeral, S. Szilagyi, J. O. Jacobus, *J. Org. Chem.* **1981**, *46*, 2082–2089.

[16] J. W. Timberlake, M. L. Hodges, K. Betterton, *Synthesis* **1972**, 632–634.

[17] The 4-(*N*,*N*-dimethylamino)phenyl, 4-methylthiophenyl, and 4-cyanophenyl derivatives of 2,5-diaryl-1,5-hexadiene, prepared from the corresponding 1,4-diarylbutane-1,4-diones, do not exhibit a clear λ_{ob} in the visible region upon LFP under similar conditions. This might be owing to low efficiencies for the cyclization of the substrate radical cations or the low efficiencies for hole transfer from $BP^{\bullet+}$ to the substrates.

[18] J. M. Dust, D. R. Arnold, *J. Am. Chem. Soc.* **1983**, *105*, 1221–1227, and references therein.

[19] M. A. O'Neill, F. L. Cozens, N. P. Schepp, *J. Am. Chem. Soc.* **2000**, *122*, 6017–6027.

[20] A value for $\lambda_{ob}(\mathbf{3a}^{+})$ of 360 nm (CF_3CH_2OH) has been reported in ref. [12b].

[21] Values for $\lambda_{ob}(\mathbf{3b}^{+})$ of 337 (HSO_3F) and 340 nm [$(CF_3)_2CHOH$] have been reported in refs. [12a] and [12b], respectively.

[22] A value for $\lambda_{ob}(\mathbf{3e}^{+})$ of 345 nm (HSO_3F) has been reported in ref. [12a].

[23] The actual relationships are as follows: $\Delta E_{ob}(\mathbf{2}^{\bullet+}) = -0.8229\sigma_c^{\cdot} - 0.028$ for $\mathbf{2a}$–$\mathbf{f}^{\bullet+}$ ($r^2 = 0.9531$), $\Delta E_{ob}(\mathbf{2}^{\bullet+}) = 0.3169\sigma^{+} + 0.0124$ for $\mathbf{2a}$–$\mathbf{d}^{\bullet+}$ ($r^2 = 0.9679$), $\Delta E_{ob}(\mathbf{2}^{\bullet+}) = -1.1185\sigma^{+} + 0.0006$ for $\mathbf{2d}$–$\mathbf{f}^{\bullet+}$ ($r^2 = 0.9994$), $\Delta E_{ob}(\mathbf{3}^{+}) = 0.5547\sigma^{+} + 0.0030$ for $\mathbf{3a}$–$\mathbf{d}^{+}$ ($r^2 = 0.9970$), and $\Delta E_{ob}(\mathbf{3}^{+}) = -2.8881\sigma^{+} + 0.0063$ for $\mathbf{3d}$–$\mathbf{f}^{+}$ ($r^2 = 0.9911$).

[24] The 4-iodophenyl derivatives $\mathbf{2g}^{\bullet+}$ and $\mathbf{3g}^{+}$ are exceptions; this is probably owing to more complex orbital interactions involving an iodine substituent.

[25] H. Namai, H. Ikeda, N. Kato, K. Mizuno, *J. Phys. Chem. A* **2007**, *111* 4436–4442.

[26] A. Rauk, *Orbital Interaction Theory of Organic Chemistry*, Wiley, New York, **1994**, Chapter 3, pp. 57–93.

[27] Consequently, the possibility of the φ_3 or $\varphi_4 \rightarrow \varphi_5$ transition of $\mathbf{2d}^{\bullet+}$ is ruled out because it cannot explain the observed reduction in the substituent effects.

[28] The orbital interaction analysis assumes that h_{AB} is almost the same in all cases. One of the reviewers suggested that this may not be true because the MOs would have a smaller coefficient on C1/C4 when a substituent is attached to the benzene ring. This assumption may be a cause of the deviation of experimental substituent effects (e.g., $E_{ob}(\mathbf{2}^{\bullet+})/E_{ob}$ $(\mathbf{3}^{+}) = 0.6$ or 0.4) from ideal substituent effects (0.5).

[29] We also performed calculations on $\mathbf{2}^{\bullet+}$ without any symmetry by using Hartree–Fock (HF) theory and obtained similar results (a chair molecular geometry and delocalized electronic structure). One of the referees commented that this is strong evidence that such a structure is indeed the correct one. ESR studies on the parent system $\mathbf{4}^{\bullet+}$ by Williams and co-workers provide direct evidence for complete delocalization: a) Q.-X. Guo, X.-Z. Qin, J. T. Wang, F. Williams, *J. Am. Chem. Soc.* **1988**, *110*, 1974–1976; b) F. Williams, Q.-X. Guo, D. C. Bebout, B. K. Carpenter, *J. Am. Chem. Soc.* **1989**, *111*, 4133–4134.

[30] Recently, Nelsen, Telo, and co-workers reported that the simple Koopmans-based model is useful for explaining the absorption spectra of *p*-phenylene-bridged intervalence radical ions: a) S. F. Nelsen, M. N. Weaver, J. P. Telo, B. L. Lucht, S. Barlow, *J. Org. Chem.* **2005**, *70*, 9326–9333; b) S. F. Nelsen, Y. Luo, M. N. Weaver, J. V. Lockard, J. I. Zink, *J. Org. Chem.* **2006**, *71*, 4286–4295; c) S. F. Nelsen, M. N. Weaver, D. Yamazaki, K. Komatsu, R. Rathore, T. Bally, *J. Phys. Chem. A* **2007**, *111*, 1667–1676.

[31] For recent studies related to pseudo-π orbitals of 1,3-biradicals, see: a) D. A. Dougherty, *Acc. Chem. Res.* **1991**, *24*, 88–94; b) W. Adam, W. T. Borden, C. Burda, H. Foster, T. Heidenfelder, M. Heubes, D. A. Hrovat, F. Kita, S. B. Lewis, D. Scheutzow, J. Wirtz, *J. Am. Chem. Soc.* **1998**, *120*, 593–594; c) M. Abe, W. Adam, W. M. Nau, *J. Am. Chem. Soc.* **1998**, *120*, 11304–11310; d) F. Kita, W, Adam, P. Jordan, W. M. Nau, J. Wirtz, *J. Am. Chem. Soc.* **1999**, *121*, 9265–9275; e) M. Abe, W. Adam, T. Heidenfelder, W. M. Nau, X. Zhang, *J. Am. Chem. Soc.* **2000**, *122*, 2019–2026; f) M. Abe, W. Adam, M. Hara, M. Hattori, T. Majima, M. Nojima, K. Tachibana, S. Tojo, *J. Am. Chem. Soc.* **2002**, *124*, 6540–6541; g) M. Abe, W. Adam, W. T. Borden, M. Hattori, D. A. Hrovat, M. Nojima, K. Nozaki, J. Wirz, *J. Am. Chem. Soc.* **2004**, *126*, 574–582.

[32] a) *Advances in Electron Transfer Chemistry* (Ed.: P. S. Mariano), JAI Press, London, **1992**; b) *Radicals, Ion Radicals, and Triplets: The Spin Bearing Intermediates of Organic Chemistry* (Ed.: N. L. Bauld), Wiley-VCH, New York, **1997**.

[33] H. Namai, H. Ikeda, Y. Hoshi, K. Mizuno, **2007**, *Angew. Chem.* **2007**, DOI: 10.1002/ange.200702512; *Angew. Chem. Int. Ed.* **2007**, DOI: 10.1002/anie.200702512.

[34] Gaussian 98, Revision A.11.4, M. J. Frisch, G. W. Trucks, H. B. Schlegel, G. E. Scuseria, M. A. Robb, J. R. Cheeseman, V. G. Zakrzewski, J. A. Montgomery, R. E. Stratmann, J. C. Burant, S. Dapprich, J. M. Millam, A. D. Daniels, K. N. Kudin, M. C. Strain, O. Farkas, J. Tomasi, V. Barone, M. Cossi, R. Cammi, B. Mennucci, C. Pomelli, C. Adamo, S. Clifford, J. Ochterski, G. A. Petersson, P. Y. Ayala, Q. Cui, K. Morokuma, D. K. Malick, A. D. Rabuck, K. Raghavachari, J. B. Foresman, J. Cioslowski, J. V. Ortiz, B. B. Stefanov, G. Liu, A. Liashenko, P. Piskorz, I. Komaromi, R. Gomperts, R. L. Martin, D. J. Fox, T. Keith, M. A. Al-Laham, C. Y. Peng, A. Nanayakkara, C. Gonzalez, M. Challacombe, P. M. W. Gill, B. G. Johnson, W. Chen, M. W. Wong, J. L. Andres, M. Head-Gordon, E. S. Replogle, J. A. Pople, Gaussian, Inc., Pittsburgh, PA, **1998**.

[35] WinMOPAC 3.9, Fujitsu Ltd., Tokyo, **2004**.

Received: May 30, 2007
Published online: September 4, 2007

